C. R. Chimie 17 (2014) 913–919

Contents lists available at ScienceDirect

Comptes Rendus Chimie

www.sciencedirect.com

Full paper/Mémoire

Oxidation of carbon black, propene and toluene on highly reducible Co/SBA-15 catalysts

Nissrine El Hassan [a,*], Samer Aouad [b], Sandra Casale [c], Henri El Zakhem [a], Hanna El Nakat [b]

[a] Department of Chemical Engineering, Faculty of Engineering, University of Balamand, PO Box 100, Tripoli, Lebanon
[b] Department of Chemistry, Faculty of Sciences, University of Balamand, PO Box 100, Tripoli, Lebanon
[c] Laboratoire de réactivité de surface, CNRS UMR 7197, Université Pierre-et-Marie-Curie, 4, place Jussieu, case courrier 178, 75252 Paris cedex 05, France

ARTICLE INFO

Article history:
Received 23 June 2013
Accepted after revision 14 October 2013
Available online 22 February 2014

Keywords:
Cobalt
Mesopores
Nanoparticles
Oxidation
SBA-15

ABSTRACT

Different cobalt loadings (3, 6, 12, 24 wt%) were impregnated using the double-solvent technique on SBA-15 calcined at 500 °C presenting a high specific surface area. The impregnated solids were stabilized at 450 °C in the air. The impregnation of cobalt led to the incorporation of cobalt oxide nanoparticles in the mesoporosity of the SBA-15. The cobalt nanoparticles were easily reducible compared to similar solids prepared by different methods. The presence of these nanoparticles enhanced significantly the reactivity of the catalysts in the considered reaction. The addition of more than 12 wt% of cobalt did not enhance the catalytic reactivity due to the deposition of cobalt oxide species on the surface of the support. The cobalt-impregnated solids are efficient in decreasing the oxidation temperature of different probe molecules and are totally selective towards the formation of CO_2 and H_2O.

Mots clés :
Cobalt
Mesopores
Nanoparticules
Oxydation
SBA-15

RÉSUMÉ

Des catalyseurs à base de cobalt (3, 6, 12, 24 % en masse) supporté sur SBA-15 ont été préparés par la méthode à deux solvant. Les solides obtenus sont stabilisés thermiquement à 450 °C à l'air. La méthode de préparation conduit à l'incorporation de nanoparticules d'oxydes de cobalt à l'intérieur des mésopores du support. Ces oxydes de cobalt sont facilement réduits par rapport à des oxydes similaires obtenus par différentes méthodes de préparation. Leur présence améliore significativement la performance catalytique des solides dans les différentes réactions d'oxydation considérées. L'ajout d'une quantité supérieure à 12 % en masse de cobalt s'est avéré inefficace du fait de la déposition des oxydes de cobalt à l'extérieur des pores. Les catalyseurs à base de cobalt contribuent à la diminution de la température d'oxydation des différentes molécules sondes avec une sélectivité totale pour la formation du CO_2 et de l'eau.

1. Introduction

Petrochemical industries emit air pollutants mainly composed of volatile organic compounds (VOCs) that are harmful to the human health and to the environment [1]. In several cases, VOCs emissions are accompanied by

* Corresponding author.
E-mail addresses: nissrine.hassan@balamand.edu.lb (N. El Hassan), samer.aouad@balamand.edu.lb (S. Aouad), Sandra.casale@upmc.fr (S. Casale), henri.elzakhem@balamand.edu.lb (H. El Zakhem), john.nakat@balamand.edu.lb (H. El Nakat).

1631-0748/$ – see front matter
http://dx.doi.org/10.1016/j.crci.2013.10.006

carbon particulates emissions (PM). The most known example is that of diesel engines [2–4]. Governments are imposing more and more strict regulations for the VOCs and PM emissions. In order to reduce these emissions, their catalytic oxidation can be used [5–8]. The noble metals catalysts show good activity [9–11], but from an economical point of view, they should be replaced by more economical types of elements, like transition metals. Among the transition metals, cobalt oxide Co_3O_4 is one of the most efficient phases in the total oxidation of VOCs [12–14]. In order to obtain a good activity of the cobalt oxide, it is important to enhance its dispersion on the support by using mesoporous silica (MCM-41, SBA-15) instead of conventional SiO_2 [15–17]. SBA-15 is more stable than MCM-41 [18], and another advantage to use SBA-15 for the oxidation of VOCs is its affinity to these molecules due to the presence of micropores [19,20], thus, permitting the fabrication of materials that are adsorbents and catalysts for the control of VOC emissions. The two-solvent method [21] can be used in order to highly disperse the cobalt oxide mainly inside the porosity of SBA-15 [22–25].

In this work, we have used the two-solvent method in order to add four different loadings of cobalt (3, 6, 12 and 24 wt %) to mesoporous silica SBA-15 and test their reactivity in the oxidation of carbon black, propene, and toluene as representatives of soot and VOCs.

2. Experimental

The SBA-15 support has been prepared according to the method described by Zhao et al. [26] with a little modification; stirring has been stopped 10 min after the addition of TEOS (Sigma–Aldrich). After a maturation of 24 h at 35 °C, the solution was filtered (rapid filtration by using a vacuum pump) and further dried at room temperature for 48 h before calcination in the air at 500 °C for 9 h with a heating rate of 2 °C/min. Calcined supports were then impregnated with a solution of cobalt nitrate (Sigma–Aldrich, ACS reagent) by following the two-solvent technique [21]. The theoretical cobalt content was varied between 3 wt% and 24 wt%. Impregnated catalysts were dried at room temperature for 24 h before being calcined under the air at 450 °C for 5 h with a heating rate of 0.5 °C/min. Catalysts are labeled as *x*-Co/SBA-15, with *x* the theoretical cobalt weight percentage.

Adsorption–desorption isotherms were recorded on ASAP 2020, Micromeritics. The samples were degassed for 2 h at 250 °C before the analyses. The BET surface areas were calculated from BET equation for a relative pressure range between 0.05 and 0.25. The microporous area was calculated by using the *t*-plot method. Mesopore size distribution was calculated by using the BJH method on both adsorption and desorption branches. X-ray diffraction measurements were performed on a Bruker D8 (λ = 1.5406 nm). A JEOL JEM-200 electron microscope operating at 200 keV (LaB_6 gun) was used; energy dispersive X-ray spectroscopy (EDXS) measurements (PGT) were carried out. Statistics were done on TEM micrographs; here, exclusively spherical particles were considered. TPR profiles were recorded on an Autochem 2920, Micromeritics. TPO (used as a pretreatment) was conducted from room temperature to 550 °C under a flow (20 mL/min) of 5 vol% O_2/He. Systematically, TPO was followed by a TPR under a flow of 5 vol% H_2/Ar (20 mL/min) from room temperature up to 1000 °C. Water was trapped by using a bath of ice and salt during TPR experiments.

The catalysts were tested in the total oxidation of propylene, toluene, and carbon black. For propylene and toluene oxidation reactions, the experiments were carried out in a conventional fixed bed microreactor between 25 °C and 400 °C (1 °C/min). The reactive flow (100 mL/min) consisted of a mixture of air and 4500 ppm of propylene or air and 1000 ppm of toluene. Before the catalytic test, the solid ($\sim$ 50 mg) was activated under a flow of air (2 L/h) at 400 °C (1 °C/min). The oxidation of carbon black CB (N330 Degussa: S_{sp} = 76 m^2/g, elementary analysis: 97.23 wt% C; 0.73 wt% H; 1.16 wt% O; 0.19 wt% N; 0.45 wt% S) was studied by simultaneous thermogravimetric (TG)–differential scanning calorimetry (DSC) analysis using a Labsys Evo apparatus. Before testing, 10 wt% of CB and 90 wt% of catalyst were grinded for 10 min using a mortar and a pestle to obtain "tight-contact" conditions. Ten milligrams of the mixture were then loaded in an alumina crucible and heated from room temperature up to 900 °C (5 °C/min) under an air flow of 50 mL/min.

3. Results and discussion

Co/Si ratios determined by EDS analyses are: 5.6; 12.9; 25.1 and 29.6 for 3-Co/SBA-15, 6-Co/SBA-15, 12-Co/SBA-15 and 24-Co/SBA-15, respectively. N_2 adsorption–desorption isotherms of all the catalysts are presented in Fig. 1A. All these isotherms are of type IV. For 3-Co/SBA-15, 6-Co/SBA-15 and 12-Co/SBA-15 catalysts, the isotherms present similar shapes with a hysteresis loop showing two distinguished parts. The first part at low pressure (P/P_0 = 0.45–0.55) corresponds to an H2 hysteresis type, while the second part at high pressure (P/P_0 = 0.55–0.7) corresponds to an H1 hysteresis type. H2 type indicates the presence of connected pores, while H1 type is more representative of a narrow pore size distribution. For the 24-Co/SBA-15 catalyst, an H2 hysteresis is only obtained in the relative pressure range of 0.45 to 0.6, indicating a complete filling and/or obstruction of the larger mesopores. The pore size distributions (BJH method), determined from the adsorption isotherms (Fig. 1B), indicate that the average pore size decreases with increasing the cobalt content. The distributions for the 3-Co/SBA-15, 6-Co/SBA-15 and 12-Co/SBA-15 catalysts (Fig. 1B) are quite similar, while that of the 24-Co/SBA-15 catalyst is shifted towards smaller pore size values. Fig. 1C shows the pore size distributions, for the different solids, obtained from the desorption isotherms. It indicates the presence of two average pore diameters for the cobalt-containing solids, the first one at 5.0 nm and the second one at 3.8 nm. The 24-Co/SBA-15 catalyst distribution indicates the presence of a porosity cantered around 3.8 nm. Table 1 lists several textural properties of the different calcined *x*-Co/SBA-15 catalysts. The surface areas decrease from 724 m^2/g to 415 m^2/g and the porous volumes decrease from 1 cm^3/g to 0.36 cm^3/g for 3 wt% and 24 wt% Co loadings, respectively.

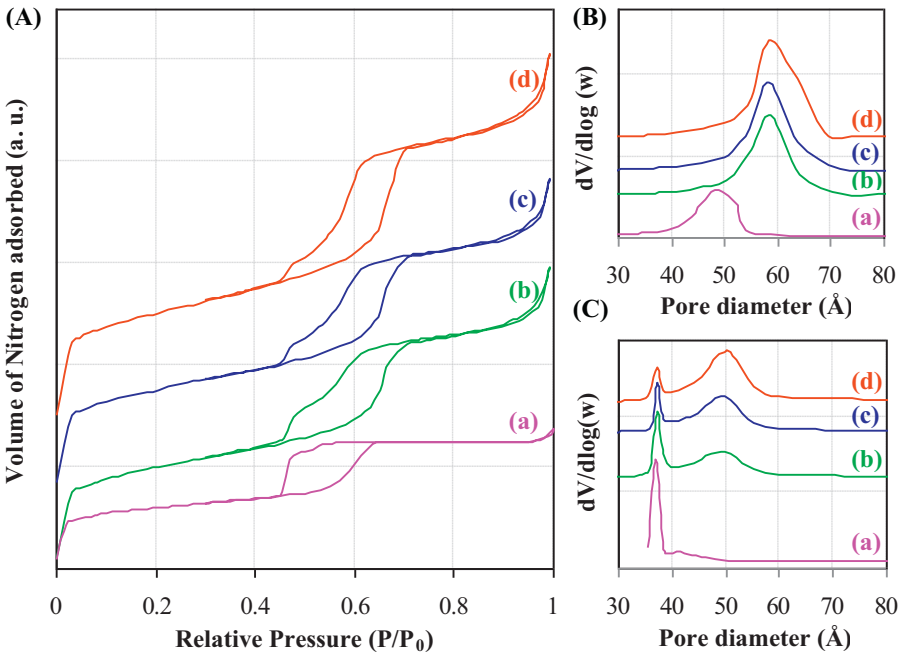

Fig. 1. (A) Adsorption–desorption isotherms and pore size distributions obtained from (B) adsorption and (C) desorption branches for (a) 24-Co/SBA-15 (b) 12-Co/SBA-15 (c) 6-Co/SBA-15 and (d) 3-Co/SBA-15.

The mesoporous area decreases according to a similar trend. It is to note that the microporous area of the 24-Co/SBA-15 catalyst is the highest among all the other catalysts. These latter observations indicate a preferential filling of mesopores rather than of micropores. The pore diameters indicate that when cobalt oxide is filling the pores, a new porosity range is created, with a maximum value around 3.8 nm. Hence, the N_2 sorption results show that the cobalt oxide species seem to fill the mesopores, but that the mesoporosity remains present, even after the addition of 24 wt% of cobalt to the SBA-15 support. Fig. 2 shows the XRD diffractograms recorded for the different cobalt-containing catalysts. The observed diffraction peaks may be attributed to the presence of Co_3O_4 (JCPDS 00-043-1003), CoO (JCPDS 01-089-2803) or Co_2SiO_4 (JCPDS 00-029-0506) species. The distinction between these three different cobalt species is impossible using the obtained XRD patterns; however, whatever their nature, the average size of the crystalline domains (based on the most intense peak) is 9.6, 13.2, 14.0, and 14.1 nm for the 3-Co/SBA-15, 6-Co/SBA-15, 12-Co/SBA-15, and 24-Co/SBA-15 catalysts, respectively. These results show that for a cobalt content $\geq$ 6 wt%, there is no effect of the cobalt loading on the crystallite size. Thus, a controlled size of the cobalt oxide species is obtained for the catalysts prepared following the two-solvent method. Fig. 3A shows the TEM micrographs obtained for the different *x*-Co/SBA-15 catalysts. The catalyst 24-Co/SBA-15 is very charged in cobalt species (Fig. 3A(a)). A partition of these species between the inside and the outside parts of the silica grains is observed. Fig. 3A(b) and A(c) show that the deposition of cobalt oxide species in the 12-Co/SBA-15 and the 6-Co/SBA-15 catalysts is similar. For instance, for the 6-Co/SBA-15 catalyst, the TEM micrograph (Fig. 3A(c)) shows a good dispersion of cobalt oxide species inside the pores along with some bigger nanoparticles outside the silica grains. These external nanoparticles are crystalline (from SAED, data not shown), but a distinction between the different cobalt varieties (Co_3O_4, CoO, and Co_2SiO_4) cannot be done. These external nanoparticles may be formed during the impregnation or may have migrated outside silica grains during the calcination. The migration hypothesis is more probable, since these nanoparticles are small and show a growth aligned with pores, which indicates a possible constraint during their crystallization and migration outside silica grains pores. For the 3-Co/SBA-15 catalyst

Table 1
Textural properties of the different *x*-Co/SBA-15 catalysts.

Catalyst	Specific surface area (m^2/g)			Pores volume (cm^3/g)	Pore diameter (nm)	
	Micro	Meso	Total S_{sp}		Adsorption	Desorption
3-Co/SBA-15	141	583	723	1.00	5.8	5.0; 3.8
6-Co/SBA-15	151	494	645	0.82	5.8	5.0; 3.8
12-Co/SBA-15	146	489	635	0.77	5.8	5.0; 3.8
24- Co/SBA-15	170	245	415	0.36	4.8	3.8

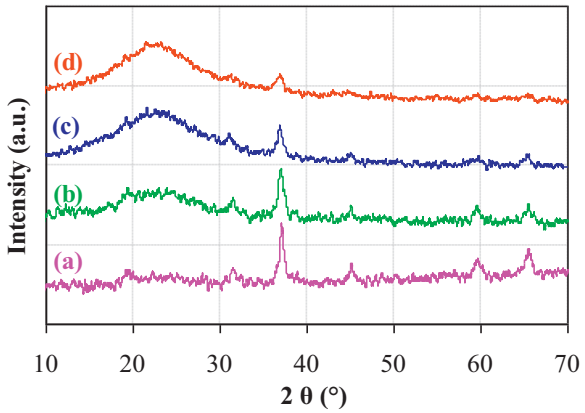

Fig. 2. XRD patterns of (a) 24-Co/SBA-15 (b) 12-Co/SBA-15 (c) 6-Co/SBA-15 and (d) 3-Co/SBA-15 catalysts.

(Fig. 3A(d)), it is observed that the majority of the cobalt oxide species are well dispersed inside the porosity of the SBA-15 support. The cobalt oxides species appear as elongated and non-spherical particles. Their small section must be smaller than that of the pores, since they are incorporated in it. The elongated shape of cobalt oxide species is in good correlation with XRD results, which showed an average crystallite size of 9.6 nm for the 3-Co/SBA-15 catalyst. From all the TEM observations, it can be concluded that a part of the cobalt species is incorporated inside the pores of SBA-15, while another part is outside the grains. A good dispersion of cobalt oxides species is observed for all the catalysts and the size of external nanoparticles remains relatively small.

To confirm this result, statistics were done on TEM images in order to determine the size distribution (Fig. 3B) and the average particle size. The particle sizes of cobalt species are within the same range; from 1 to 15 nm; for the 3-Co/BA-15; 6-Co/SBA-15 and 12-Co/SBA-15. The average particle sizes for these catalysts are: 5.0, 6.2 and 3.9 nm. From the sizes, one can clearly see that the majority of cobalt species are located inside the pores with a fraction outside the porosity (larger than 6 nm). For the 24-Co/SBA-15 catalyst, the size distribution is large (from 4 to 33 nm) and the average size is 18.2 nm. This result clearly shows the presence of larger particles outside the pores for high cobalt contents. It is worth noting that the difference observed between the average size of the last catalyst determined by XRD and TEM can be attributed to the presence of small nanoparticles difficult to see on TEM images in the presence of large external particles.

The reduction profiles of the different catalysts are presented in Fig. 4. The profile of the 3-Co/SBA-15 catalyst shows different reduction peaks cantered at 204, 317, 432, 648, and 868 °C. The first small contribution is generally assigned to the reduction of clusters of cobalt species, while the first and second peaks are attributed to the reduction of Co_3O_4 in two steps [27,28]. The first step corresponds to the reduction of CoIII and the second one to the reduction of CoII. The second peak is generally attributed to the reduction of CoII ions [29,30], while the third one is that of the reduction of cobalt silicate [31].

The reduction behaviours of the other samples are similar to that of the first catalyst, except the first peak, which is not present for these catalysts. The different reduction regions are indicated by 1, 2 and 3, and their relative proportions are summarized in Table 2. For the catalyst 6-Co/SBA-15, the percentages of Co_3O_4 and CoII are quite similar, with a negligible percentage of cobalt silicate, which can be correlated with the negligible presence of very small cobalt species (from 1 to 3 nm), as it can be seen in Fig. 3B(c). It should be noted that the position of the peaks shifts from one catalyst to another one. This can be attributed to the size of particles to reduce, for example, on the 6-Co/SBA-15, the reduction of Co_3O_4 occurs at a lower temperature than on the other catalyst. As mentioned before, this catalyst does not contain small nanoparticles, so, reduction is taking place more easily.

For the catalyst 12-Co/SBA-15, the percentages of Co_3O_4 and CoII are 46.9 and 48.6%, with a little fraction of cobalt silicate (4.5%). On the latter catalyst, 24-Co/SBA-15, these percentages are 54.2, 37.3, and 8.5%. For all these catalysts, the cobalt silicate has a minor contribution to the TPR profiles and the two main species are Co_3O_4 and CoII. This indicates that these catalysts are more reducible than Co/SBA-15 prepared in similar conditions, with a difference in SBA-15 drying.

Fig. 5 shows the parameter $T_{20\%}$, which represents the temperature at which 20% of the carbon black, propylene or toluene is converted in the presence of *x*-Co/SBA-15 solids. The $T_{20\%}$ value is chosen for catalytic comparison, as at this conversion rate, the reactions are under catalytic control and relative performances can be compared. The $T_{20\%}$ temperature for non-catalyzed carbon black oxidation is 629 °C. SBA-15 decreases this temperature to 500 °C. Following the impregnation of 3 wt% of cobalt on the support, the $T_{20\%}$ parameter for carbon black oxidation was lower than that for the support alone. Thus, the presence of cobalt oxide species favours carbon black oxidation at lower temperatures. It is observed that for cobalt loadings $\geq$ 12 wt%, there is no significant enhancement of the catalytic activity in carbon black oxidation, as $T_{20\%} \sim 300$ °C for both 12-Co/SBA-15 and 24-Co/SBA-15 catalysts. Similar results are observed in both propylene and toluene oxidation reactions. In fact, the addition of a small amount of cobalt (3 wt%) showed a considerable decrease in $T_{20\%}$. This decrease is about 114 °C and 67 °C for propylene and toluene, respectively. Moreover, an additional decrease was observed for higher cobalt contents, but the enhancement in the catalytic activity was non-significant when more than 12 wt% cobalt were

Table 2
Relative percentages of the different cobalt oxide species obtained from the analysis of the TPR profiles.

Catalyst	Peak area percentage relatively to the total peak area (%)		
	Co_3O_4 Peak 1	C^{II} ions species Peak2	Cobalt silicates Peak 3
3-Co/SBA-15	60.7	33.7	5.5
6-Co/SBA-15	52.5	46.3	1.2
12-Co/SBA-15	46.9	48.6	4.5
24-Co/SBA-15	54.2	37.3	8.5

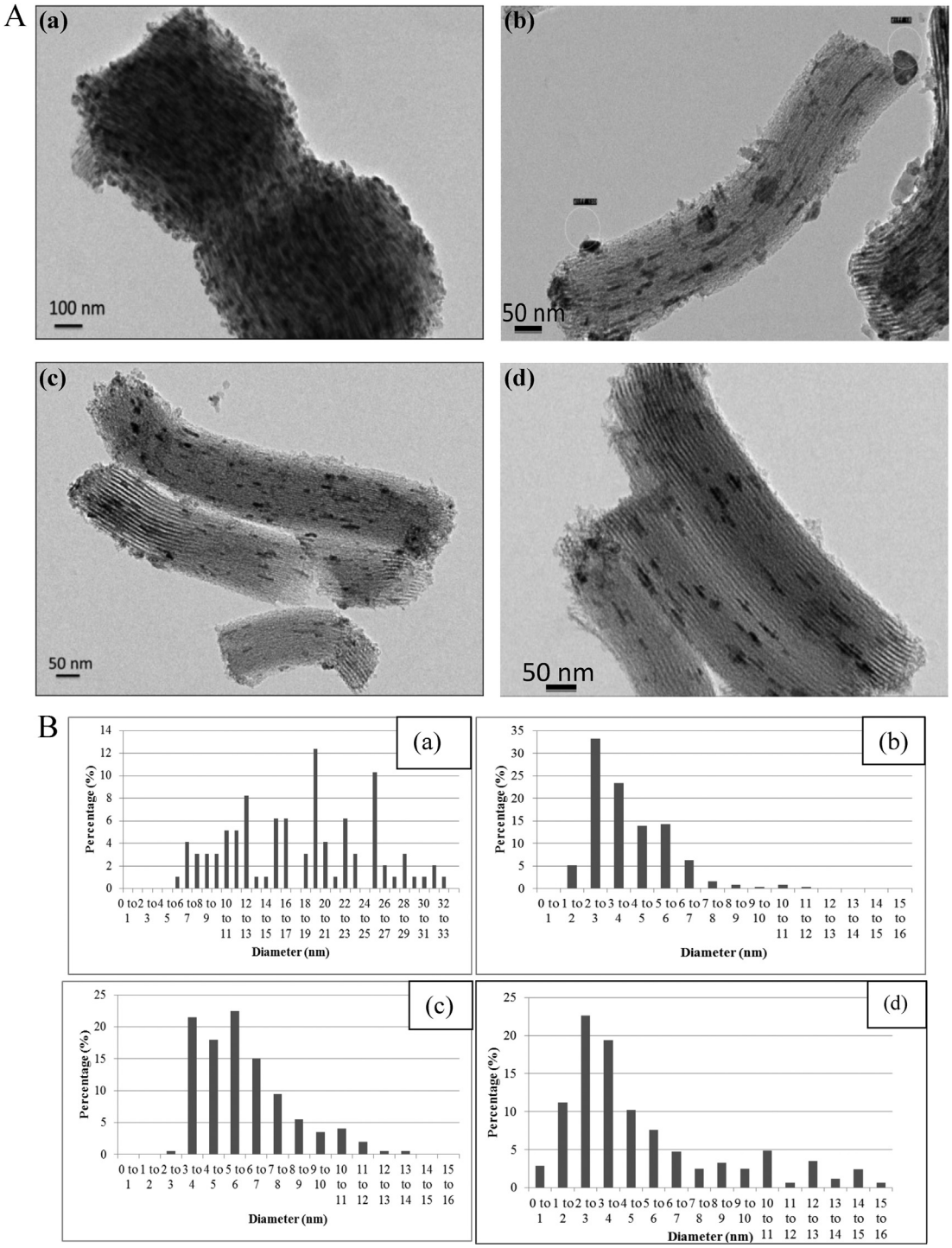

Fig. 3. A. TEM micrographs of (a) 24-Co/SBA-15 (b) 12-Co/SBA-15 (c) 6-Co/SBA-15 and (d) 3-Co/SBA-15 catalysts. B. Particle size distribution of (a) 24-Co/SBA-15 (b) 12-Co/SBA-15 (c) 6-Co/SBA-15 and (d) 3-Co/SBA-15 catalysts.

impregnated on the SBA-15 support. The insert in Fig. 5 plots the $T_{20\%}$ parameter versus the Co/Si ratio obtained from EDS analyses. The temperature decreases in a perfect linear manner for the two gaseous reactants. The decrease is not linear for CB oxidation; however, it is clear from the insert that it is the amount of cobalt species that are present inside the mesopores that correlate better with the catalytic reactivity in the considered oxidation reactions. According to the above results, it can be suggested that with the used impregnation method, cobalt oxide species begin to fill the SBA-15 mesopores with a part being deposited outside the porosity. The species inside the

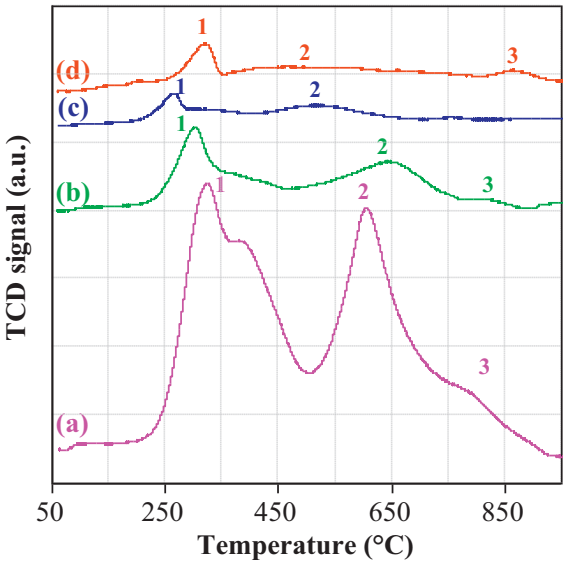

Fig. 4. TPR profiles of (a) 24-Co/SBA-15 (b) 12-Co/SBA-15 (c) 6-Co/SBA-15 and (d) 3-Co/SBA-15 catalysts.

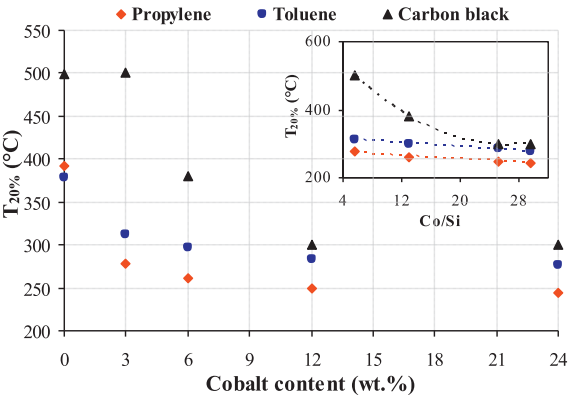

Fig. 5. Effect of the cobalt content in *x*-Co/SBA-15 catalysts on $T_{20\%}$ in propylene, toluene, and carbon black oxidation reactions. Insert: $T_{20\%}$ versus Co/Si ratio in the mesopores.

pores are more beneficial than those deposited outside, since the pores structure promote the formation of cobalt oxides nanoparticles and provide longer contact times between the catalytic sites and the reactants. This is in line with the observed catalytic results, as for 12 wt% cobalt the Co/Si for areas with incorporated nanoparticles ratio is 25% and it just increases to 29.5% for 24 wt% cobalt. Moreover, increasing the cobalt content from 12 wt% to 24 wt% leads to a drastic decrease in the mesoporous area. Therefore, the increased number of cobalt oxides species was offset by the decreased mesoporous area. Finally, it is also probable that the number of active sites present for cobalt loadings of 12 wt% is sufficient to reach maximum turnover rates with the different probe molecules (carbon black, propylene and toluene) making additional cobalt addition inefficient. These results show that, even if the catalytic reactivity is usually affected by the specific surface area of the solid, the position (inside or outside pores) of the active catalytic site is more important in determining the performance of a catalyst. In fact, the catalytic reactivity depends on the structural properties of the cobalt oxides species. It is worth mentioning that CO and CO_2 selectivities were monitored in both reactions and were found to be equal to 0% and 100% respectively, whatever the solid used.

In order to monitor the changes occurring during the reaction (propene oxidation), the spent 12-Co/SBA-15 catalyst was characterized by N_2 sorption, XRD, and TEM. The surface area of the spent catalyst is 484 m^2/g; with a mesoporous and microporous areas of 336 and 148 m^2/g, respectively. This result indicates that the microporous area remains the same after the oxidation of propene, but a decrease of 31% of the mesoporous area has occurred. No change in the nature of the active phase or of the Co_3O_4 corresponding peaks was detected by XRD. From TEM images (Fig. 6), it can be clearly seen that a migration of the active phase has occurred; this is confirmed by the

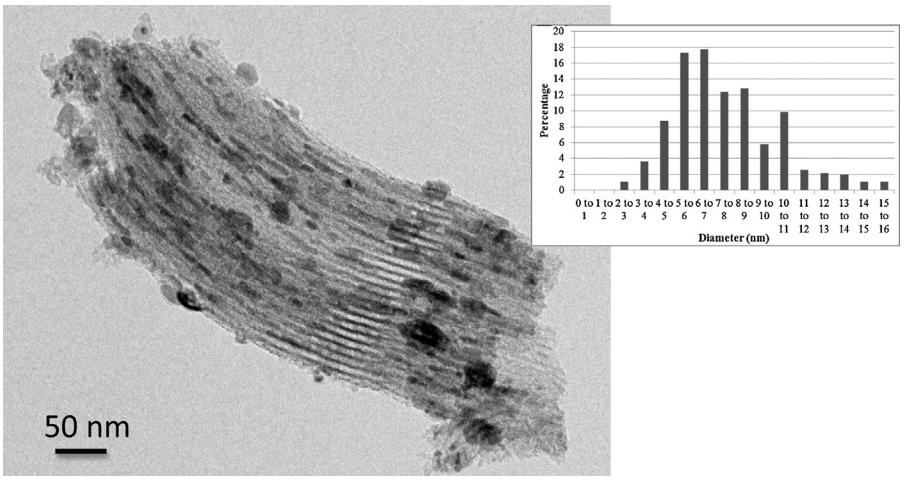

Fig. 6. TEM micrograph of spent 12-Co/SBA-15 with particle size distribution.

statistics done, where the average size of the particles has increased from 3.9 to 7.8 nm. No coke has been detected on TEM images, by EDS analyses, and XRD.

4. Conclusion

A high dispersion of cobalt oxides on SBA-15 was obtained on the different catalysts prepared by the two-solvent method. A great part of these oxides was deposited inside the porosity, but the fraction of external particles increased with increasing the cobalt content. It seems that the catalytic activity toward CB, propene and toluene oxidations is enhanced by the presence of the active phase inside the support; there is no important contribution of external particles in the catalytic activity.

Acknowledgements

The authors thank the "Traitement catalytique et énergie propre" group at the UCEIV, ULCO, Dunkerque, France, for their help in the toluene oxidation test. Special thanks are addressed to Mr. Makram El Bachawati, Mr. Bilal El Khoury and Ms. Hala Fallah for their technical support. Authors would also like to thank the University of Balamand Research Council for financial support through the BIRG 18/2010 and the Lebanese University (Hadath Campus) for the XRD experiments.

References

[1] K. Everaert, J. Baeyens, J. Hazard. Mater. 109 (2004) 113.
[2] H. Schulz, G. Bandeira De Melo, F. Ousmanov, Combust. Flame 118 (1999) 179.
[3] T. Schmitz, D. Hassel, F.J. Weber, Atm. Environ. 34 (2000) 4639.
[4] B.T. Jobson, M.L. Alexander, G.D. Maupin, G.G. Muntean, Int. J. Mass Spectrom. 245 (2005) 78.
[5] M. Iamarino, P. Salatino, R. Chirone, R. Pirone, G. Russo, Proc. Combust. Inst. 29 (2002) 827.
[6] S. Aouad, E. Abi-Aad, A. Aboukaiss, Appl. Catal. B: Environ. 88 (2009) 249.
[7] A. Szegedi, M. Popova, C. Minchev, J. Mater. Sci. 44 (2009) 6710.
[8] J.M. Jones, L.I. Darvell, T.G. Bridgeman, M. Pourkashanian, A. Williams, Proc. Combust. Inst. 31 (2007) 1955.
[9] S. Ivanova, C. Petit, V. Pitchon, Gold Bull. 39 (2006) 3.
[10] A.C. Gluhoi, N. Bogdanchikova, B.E. Nieuwenhuys, J. Catal. 232 (2005) 96.
[11] T. Maillet, C. Solleau, J Barbier Jr., D. Duprez, Appl. Catal. B: Environ. 14 (1997) 85.
[12] T.V. Choudhary, S. Banerjee, V.R. Choudhary, Appl. Catal. A: Gen. 234 (2002) 1.
[13] V.R. Choudhary, G.M. Deshmukh, Chem. Eng. Sci. 60 (2005) 1575.
[14] T. Garcia, S. Agouram, J.F. Sanchez-Royo, R. Murillo, A.-M. Mastral, A. Aranda, I. Vazquez, A. Dejoz, B. Solsona, Appl. Catal. A: Gen. 386 (2010) 16.
[15] Y. Khodakov, R. Bechara, A. Griboval-Constant, Appl. Catal. A 254 (2003) 273.
[16] J. Kim, B.C. Dunn, P. Cole, G. Turpin, R.D. Ernst, R.J. Pugmire, M. Kang, J.M. Kim, E.M. Eyring, Chem. Commun. (2005) 1462.
[17] A.P. Katsoulidis, D.E. Petrakis, G.S. Armatas, P.N. Trikalitis, P.J. Pomonis, Micropor. Mesopor. Mater. 92 (2006) 71.
[18] M.T. Bore, H.N. Pham, E.E. Switzer, T.L. Ward, A. Fukuoka, A.K. Datye, J. Phys. Chem. B 109 (2005) 2873.
[19] D.P. Serrano, G. Calleja, J.A. Botas, F.J. Gutierrez, Ind. Eng. Chem. Res. 43 (2004) 7010.
[20] K. Kosuge, S. Kubo, N. Kikukawa, M. Takemori, Langmuir 23 (2007) 3095.
[21] M. Imperor-Clerc, D. Bazin, M.D. Appay, P. Beaunier, A. Davidson, Chem. Mater. 16 (2004) 1813.
[22] I. Lopes, N. El Hassan, H. Guerba, G. Wallez, A. Davidson, Chem. Mater. 18 (2006) 5826.
[23] G. Laugel, J. Arichi, H. Guerba, M. Moliere, A. Kiennemann, F. Garin, B. Louis, Catal. Lett. 125 (2008) 14.
[24] F. Boubekr, A. Davidson, S. Casale, P. Massiani, Microp. Mesopor. Mater. 141 (2011) 157.
[25] J. Taghavimoghaddam, G.P. Knowles, A.L. Chaffee, Top. Catal. 55 (2012) 571.
[26] D. Zhao, J. Feng, Q. Huo, N. Melosh, G.H. Fredrickson, B.F. Chmelka, G.D. Stucky, Science 279 (1998) 548.
[27] H. Li, J. Li, H. Ni, D. Song, Catal. Lett. 110 (2006) 71.
[28] H. Xiong, Y. Zhang, K. Liew, J. Li, Fuel Process. Technol. 90 (2009) 237.
[29] G. Bagnasco, M. Turco, C. Resini, T. Montanari, M. Bevilacqua, G. Busca, J. Catal. 225 (2004) 536.
[30] N. El Hassan, PhD thesis, Université Pierre-et-Marie-Curie, Paris, France, 2008
[31] T. Vralstad, H.K. Magnusson, J. Sjoblom, Micropor. Mesopor. Mater. 106 (2007) 155.